Polymer 226 (2021) 123813

Contents lists available at ScienceDirect

Polymer

journal homepage: www.elsevier.com/locate/polymer

Stability of particle dispersion and heterogeneous interfacial layers in polymer nanocomposites

Chen Gong [a,b], Donovan Weiblen [a,b], Deniz Rende [b], Pinar Akcora [c], Rahmi Ozisik [a,b,*]

[a] Department of Materials Science and Engineering, Rensselaer Polytechnic Institute, Troy, NY, 12180, USA
[b] Center for Materials, Devices, and Integrated Systems, Rensselaer Polytechnic Institute, Troy, NY, 12180, USA
[c] Department of Chemical Engineering and Materials Science, Stevens Institute of Technology, Hoboken, NJ, 07030, USA

ARTICLE INFO

Keywords:
Polymer nanocomposite
Heterogeneous interface
Extrusion

ABSTRACT

In a groundbreaking study, Akcora group has shown that poly(ethylene oxide), PEO, nanocomposites with dynamically asymmetric, heterogeneous interfaces present a unique and reversible thermal-stiffening behavior above the glass transition temperature of the adsorbed polymer (Senses, E. et al., *ACS Appl. Mater. Interfaces* **2015**, *7*, 14682–14689.). However, chemically heterogeneous interfaces can be fragile under severe shear fields that are common in continuous polymer processes. The current study is inspired by the work done in Akcora group on thermally-stiffening polymer nanocomposites and is aimed at understanding the effect of continuous processing operations such as extrusion on the structure and properties of thermally-stiffening nanocomposites. The effect of processing on nanocomposites of PEO and colloidal silica, SiO_2, were investigated via thermogravimetric analysis (TGA), scanning electron microscopy (SEM), small and wide angle X-ray scattering, attenuated total reflectance-Fourier transform infrared (ATR-FTIR), and rheometry. Three types of silica nanoparticles were employed in the current study (while keeping the average silica nanoparticle size and concentration constant: 40–50 nm diameter and 30% by weight): bare silica, silica adsorbed with polycarbonate (PC), and silica adsorbed with poly(2–vinyl pyridine), P2VP. The adsorption of PC and P2VP onto silica creates a dynamically asymmetric, heterogeneous interface that is quite different compared to homogeneous interfaces where either nanoparticle surfaces are chemically modified with small chemical groups or with long grafted chains. The results indicated that upon extrusion, the average size of secondary agglomerates either remained unchanged or decreased slightly but the amount of agglomeration increased leading to deterioration of silica nanoparticle dispersion and viscoelastic properties (at temperatures below the glass transition temperature of the adsorbed polymer). Among the three systems studied, P2VP-adsorbed silica containing samples showed the largest degradation of viscoelastic properties upon extrusion, which was attributed to the desorption and disentanglement within the heterogeneous interface or to agglomeration leading to breaking of the percolated structure formed by nanoparticles and polymer bridges.

1. Introduction

Over the last few decades, polymer nanocomposites have drawn much attention both from industry and academy due to their superior and tailorable performance [1–6]. The volume fraction of chains in close proximity of the nanofiller (commonly referred to as the "interface") increases with decreasing nanofiller size and increasing nanofiller concentration. And polymer chains at the interface region have been shown to have significantly altered conformations and dynamics compared to those in the bulk [7–11]. As a result, it is common to have the properties of the whole nanocomposite be dominated by those of the interface. Given the crucial role interfaces play on the overall properties of polymer nanocomposites, it is of utmost importance to understand the structure and properties of the interface. However, in most cases, these studies have been focused on homogeneous interfaces [12–14] and little attention has been paid to heterogeneous interfaces [15]. For example, there have been extensive and systematic studies on homogeneous interfaces with the goal of controlling the overall macroscopic properties of the composite by manipulating the structure of the interface, matrix polymer-nanofiller interactions, and state of nanofiller dispersion and distribution [1,15,16]. The structure of heterogeneous interfaces is more complicated and is strongly dependent on the matrix polymer and the

* Corresponding author. 110 8th Street, MRC-205, Rensselaer Polytechnic Institute, Troy, NY, 12180, USA.
E-mail address: ozisik@rpi.edu (R. Ozisik).

https://doi.org/10.1016/j.polymer.2021.123813
Received 5 December 2020; Received in revised form 31 March 2021; Accepted 22 April 2021
Available online 26 April 2021

polymer physically adsorbed or chemically grafted to the nanofiller. Most importantly, in the case of nanocomposites with heterogeneous interfaces, the miscibility of the nanofillers and the matrix polymer, which is generally controlled by entropic effects in nanocomposites with homogeneous interfaces, is largely controlled by enthalpic effects between the matrix and adsorbed/grafted polymers. These enthalpic interactions within the heterogeneous interfaces are further complicated by the curved geometry of the heterogeneous interface [8,17]. Recent studies by Akcora group on polymer nanocomposites with dynamically asymmetric, heterogeneous interfaces showed how these new class of nanocomposites can lead to unique and unusual properties. Poly (ethylene oxide), PEO, and colloidal silica (SiO_2) nanocomposites, where the silica nanoparticles were modified by physically adsorbing high-glass-transition-temperature polymers such as poly(methyl methacrylate), PMMA, demonstrated a unique and reversible thermal-stiffening behavior at temperatures above the glass transition temperature (T_g) of the adsorbed polymer [18]. Thermal-stiffening in the PEO–SiO_2–PMMA system was attributed to the dynamic asymmetry of chains at the interphase region around nanoparticles. It was subsequently shown that the dynamic heterogeneity led to faster reptation dynamics of PEO chains within the interface when the adsorbed chains are glassy at temperatures below the T_g of the adsorbed chains [19], and the faster reptation at the interface was attributed to the disentanglement of PEO chains when they are confined within the glassy adsorbed PMMA chains. At temperatures above the T_g of the adsorbed PMMA, PEO chains were found to be dynamically coupled to the PMMA chains, which were in the rubbery state [20–22].

The current work is inspired by recent studies in polymer nanocomposites with dynamically asymmetric, heterogeneous interfaces. The goal of the current study is to understand the effect of common processing methods such as extrusion on the structure and properties of PEO–SiO_2 nanocomposites with dynamically asymmetric, heterogeneous interfaces. Extrusion is one of the most fundamental processing techniques used in the processing of polymers and forms the basis of many other processing operations [23,24]. Unlike the well-defined large amplitude shear deformation experiments performed in previous studies [22], the shear fields that are encountered inside an extruder can be chaotic and might lead to permanent changes in the state of nanoparticle dispersion and distribution due to the severe particle-particle collisions [25]. In addition, although many processing-structure-property models has been established for polymers, their applicability to polymer nanocomposites with heterogeneous interfaces has not been explored [13,26–28].

In the current study, the effect of shear rate during extrusion on PEO–SiO_2 polymer nanocomposites with two different adsorbed polymers were investigated by employing various characterization methods such as thermogravimetric analysis (TGA), wide and small angle X-ray scattering (WAXS, SAXS), scanning electron microscopy (SEM), attenuated total reflectance-Fourier transform infrared (ATR-FTIR) spectroscopy, and strain controlled oscillatory rheology. The two adsorbed polymers were polycarbonate (PC) and poly(2–vinyl pyridine), P2VP. Results were compared to PEO composites containing bare silica, and neat PEO. In a previous study that employed large deformations (>100% strain), PEO-SiO_2–PMMA and PEO–SiO_2–P2VP were found to display very different viscoelastic responses that were attributed to the disentanglement and desorption events within the PEO–P2VP interfaces [21] due to the rigidity of the adsorbed P2VP chains. Therefore, PC and P2VP were selected as the adsorbed polymers due to their different T_gs and chain rigidities.

2. Experimental

2.1. Materials

Hydroxyl terminated poly(ethylene oxide), PEO, at 100 kDa was used as the matrix polymer in all composite samples. Colloidal silica (SiO_2) with nominal diameter of 40–50 nm (as reported by the manufacturer) dispersed in 2-butanone (MEK) was purchased from Nissan Chemical American Corporation and used as received. Two different polymers were chosen as surface modifiers for silica (see Table 1): poly (2-vinyl pyridine), P2VP, with an average molecular weight of 40 kDa (Polysciences Inc.) and poly(bisphenol A carbonate), PC, with an average molecular weight of 45 kDa (Sigma Aldrich). Both P2VP/PEO and PC/PEO blends present a low critical solution temperature (LCST) behavior, and the low bounds are both higher than the operating temperature in this work [29,30].

All polymeric samples were used after drying in vacuum oven at 40 °C for 24 h. Solvents including toluene, 2-butanone, tetrahydrofuran (THF), acetone, dichloromethane (DCM), and ethanol were purchased from Sigma Aldrich, and they were used as received.

2.2. Nanocomposite sample preparation procedure

The following procedure was adopted to prepare bulk nanocomposites containing surface modified silica nanoparticles: (i) each polymer was dissolved in an appropriate solvent (P2VP in THF, PC in DCM) at a concentration of 30 mg/mL, (ii) 1.07 mL of silica suspension was added to 25 mL of P2VP/THF or PC/DCM solution at room temperature, (iii) the combined solution was sonicated for 30 min followed by 2 h of vigorous stirring to fully disperse silica nanoparticles, (iv) solutions were then ultra-centrifuged three times at 11,000 rpm for 60 s at room temperature to separate polymer–adsorbed silica nanoparticles from the solvent, (v) polymer–adsorbed silica nanoparticles were mixed with 15 mL of PEO solution with a concentration of 25 mg/mL, and were vigorously stirred until the solution is clear to the eye, (vi) then the mixture was poured into a polytetrafluoroethylene (PTFE) Petri dish, and was left in a vacuum hood for 24 h to remove the solvent, (vii) the dried nanocomposite disc was annealed at 90 °C in vacuum oven for 48 h to reach quasi-equilibrium configuration.

The concentration of modified nanoparticles was kept fixed at 30% by weight (~17% by volume, φ), which is beyond the hydrodynamic limit [2]. The average interparticle surface-to-surface distance (h) is estimated by assuming a random distribution of nanoparticles having an average radius r of 22.5 ± 2.5 nm (see Eq. (1) [19]). The estimated h of 24.9 ± 2.8 nm is greater than the radius of gyration of PEO, hence the chain confinement does not play a significant role on the polymer nanocomposites discussed in the current work.

$$h = r\left[\left(\frac{16}{\pi\varphi}\right)^{1/3} - 2\right] \tag{1}$$

2.3. Thermogravimetric analysis

Thermogravimetric analysis (TGA) was carried out using a TA Instrument Q50 at a heating rate of 20 °C/min up to 580 °C. Thermograms were analyzed to calculate the approximate amount of adsorbed polymer chains on silica nanoparticles.

Table 1
Basic characteristics of the materials used in the current study.

	T_g (°C)	C_∞	R_g (nm)	γ (mN/m)	γ^d(mN/m)	γ^p(mN/m)
PEO	−65	6.7	17.08	43.0	30.9	12.0
P2VP	94	10.0	5.40	39.5	29.8	9.7
PC	152	9.4	8.06	34.2	27.7	6.5
SiO_2 [31–33]	–	–	–	70.3–77.7	9.2–38.9	31.4–68.1

T_g is the glass transition temperature; C_∞ is the characteristic ratio; R_g is the radius of gyration; and γ γ^d, and γ^p are the total surface energy, dispersive component of the surface energy, and polar component of the surface energy, respectively.

2.4. Extrusion procedure

Neat PEO, PEO/SiO_2, and PEO/SiO_2–adsorbed polymer nanocomposites were extruded using a laboratory mixing extruder (Dynisco Inc.) at 80 °C and at two different screw speeds: 30 and 90 rpm. Extrusion was conducted under nitrogen protection to minimize thermal degradation and processing (residence) times were approximately 4–5 min for each sample. The extrudates coming out of the die were collected and processed into different shapes for further characterization. Nanocomposite samples were designated as following: PEO–SiO_2–[adsorbed polymer]–[screw speed in rpm]. For example, PEO–SiO_2–P2VP–30 stands for the sample having PEO as the matrix polymer, P2VP–adsorbed silica nanoparticles as reinforcing agents, and was processed at a screw speed of 30 rpm.

2.5. Scanning electron microscopy

Samples were put into liquid nitrogen for 2 h before broken by a sharp awl to create a smooth surface. After sputtered with Ag/Pd gas mixture, samples were analyzed using FEI VERSA 3D dual beam field emission/low vacuum scanning electron microscope (SEM). The voltage was fixed at 5.00 kV, and the work distance was kept at ~10 mm. Multiple SEM images were obtained at different locations and at varying magnifications.

2.6. Small and wide angle X–ray scattering

Small angle X-ray scattering (SAXS) experiments were performed at Beamline 12ID from the National Synchrotron Light Source (NSLS), Brookhaven National Laboratory with an X-ray source having a wavelength of 0.889 Å corresponding to an energy of 13950.01 eV. The distance between sample and detector was 8.3 m, and the pixel size was 0.172 mm. Each measurement took 0.25 s. The resulting data (in the q range of 0.003–0.1 $Å^{-1}$), which was corrected for background, was reduced to 2D using Igor Pro/Nika software package [34,35], and subsequently fitted by a two-level Unified model using the Igor Pro/Irene software package [36–38]. Wide angle X-ray scattering (WAXS) results were obtained simultaneously during the SAXS experiments. JADE software package was used to calculate polymer crystallinity from WAXS data [39].

2.7. Attenuated total Reflectance–Fourier transform infrared spectroscopy

Attenuated total reflectance-Fourier transform infrared (ATR-FTIR) spectra was collected from 10 scans with a Nicolet iS50 FTIR spectrometer (Thermo Fisher Scientific Co.) in the range of 400–4000 nm^{-1}. A diode laser with a wavelength of 1064 nm was used as the source. Data was collected by a single-bounce diamond crystal detector. All the experiments were performed at room temperature. OMNIC software package was used for advanced ATR correction, baseline correction, and smoothening. The resulting data was analyzed using Origin software package for peak-differentiating and peak-imitating.

2.8. Viscoelastic characterization

The linear viscoelastic properties of neat PEO and PEO nanocomposites at room temperature and 85 °C were measured by a strain-controlled AR-G2 rheometer (TA Instruments). Rheological measurements were all carried out under N_2 protection. The nanocomposite samples were first cut into small pieces and then hot-pressed at 80 °C into 1-mm-thick discs to fit into the 8-mm-diameter stainless steel parallel plates of the rheometer. Both temperature and frequency sweeps were performed in the linear regime, which was previously determined by performing a linear strain-stress test. Samples were placed between the rheometer plates, then they were heated to 85 °C and were kept at this temperature for 5 min to melt samples before measurement. Frequency sweep tests were performed from 100 to 0.01 rad/s and 10 data points were collected per decade.

3. Results and discussion

Numerous studies including both simulations and experiments have been performed to understand the effect of interfacial energetics and processing condition on dispersion [13,27]. It is well established that the ratio of the work of adhesion between polymer and filler (w_{PF}) to the work of adhesion between filler and filler (w_{FF}) is an important indicator in predicting the nanoparticle dispersion propensity after processing [40]. If $w_{PF}/w_{FF} < 1$ (equivalent to having a contact angle greater than 0°), the filler would prefer to decrease its surface energy by establishing contacts with other fillers instead of the host polymers. In this situation, nanoparticles will tend to agglomerate and the whole system will have a poor dispersion. The work of adhesion ratio (w_{PF}/w_{FF}) and contact angle (θ) can be calculated from the surface energies as follows:

$$1+\cos\theta = 2\left(\frac{W_{PF}}{W_{FF}}\right) = 2\left(\frac{\sqrt{\gamma_P^d\gamma_F^d}+\sqrt{\gamma_P^p\gamma_F^p}}{\gamma_F}\right) \quad (2)$$

where γ_P^d and γ_F^d are the dispersive components of the polymer and filler surface energies, respectively; γ_P^p and γ_F^p are the polar components of the polymer and filler surface energies, respectively; γ_F is the surface energy of the filler ($\gamma_F = \gamma_F^d + \gamma_F^p$) [41]. Using w_{PF}/w_{FF} as a descriptor works well in many binary nanocomposite systems, even in nanocomposites containing silane–modified silica nanoparticles [13,42]. In terms of the effect of processing condition, it was argued that the dispersion quality can be improved with increasing mixing energy irrespective of interfacial energetics [43].

In the current study, the work of adhesion ratio between silica and PEO was calculated to be ~0.769 according to the data shown in Table 1, and given that this value is less than unity, silica nanoparticles should form agglomerates after extrusion. As a comparison, the work of adhesion ratios for SiO_2–P2VP and SiO_2–PC were calculated to be ~0.733 and 0.670, respectively. These values are less than that of SiO_2–PEO, therefore, it is expected that nanofillers will form agglomerates in these composites as well. However, in the current study, we do not have composites of silica with P2VP and PC but rather, we have composites of P2VP– and PC–adsorbed silica nanofillers with PEO, therefore, in addition to SiO_2–P2VP and SiO_2–PC interfaces, we also have PEO–P2VP and PEO–PC interfaces that might alter the dispersion state of silica nanoparticles. For example, the work of adhesion ratios for PEO–P2VP and PEO–PC were calculated to be 1.041 and 1.114, respectively (assuming P2VP and PC to be the solid phases within PEO). These values suggest that P2VP and PC would prefer to be dissolved with the PEO matrix.

The work of adhesion ratio analysis suggests the possibility of an interesting interplay for the P2VP– and PC–adsorbed SiO_2 nanocomposites. In these systems, while silica nanoparticles have low work of adhesion ratios (<1.0) with P2VP and PC compared to PEO, PEO has high work of adhesion ratios (>1.0) with P2VP and PC. Therefore, according to work of adhesion calculation, there is a possibility that silica nanoparticles would be well dispersed by extrusion because although silica nanoparticles want to agglomerate to lower their surface energy, PEO tends to mix with the adsorbed high-T_g polymers, essentially creating a pressure against silica agglomeration. In addition, since the adsorbed polymers (P2VP and PC) have high glass transition temperatures, they would act as solid barrier/cage (while being porous to PEO) preventing silica nanoparticles to interact with each other. Based on the work of adhesion ratio analysis and due to the nature of solution processing methodology employed, we hypothesize that solution mixed nanocomposites will show good dispersion of silica nanofillers after extrusion.

One might propose that processing these nanocomposites in an extruder at temperatures less than the T_gs of the adsorbed polymers might not have any effect on the state of nanofiller dispersion. However, during processing, PEO chains would diffuse into the adsorbed polymer domain and lower the effective T_g at the adsorbed layer, and thereby, enabling the nanofillers to diffuse out of the adsorbed polymer cage and form agglomerates [21]. The extent of nanofiller agglomeration upon processing is one of the main goals of the current study. But in order to obtain a clear understanding of the role of adsorbed polymers on the state of nanofillers dispersion and on the overall properties, it is necessary to understand the characteristics of the adsorbed P2VP and PC layers on silica nanoparticles.

3.1. Characterization of adsorbed nanoparticles

P2VP or PC adsorbed nanoparticles were prepared via solution mixing as described previously. The amount of absorbed polymer was determined via Thermal Gravimetric Analysis (TGA). The results for P2VP and PC adsorbed silica nanoparticles are shown in Fig. 1. The adsorbed amounts of P2VP and PC were found to be ~3.2 and ~0.45% (by weight), respectively. These correspond to ~32.3 P2VP and ~4.0 PC chains per silica nanoparticle. The bulk densities of P2VP and PC are 1.14 and 1.22 g/cm^3, respectively, therefore, if we assume that the adsorbed layers have the same densities as those in the bulk, the adsorbed layer thicknesses are calculated to be 0.37 nm for P2VP and 0.049 nm for PC for a nanoparticle with an average radius of 20 nm and density of 2.0 g/cm^3. However, it should be noted that the estimation of adsorbed layer thicknesses from TGA was shown to result in underestimation of the real layer thickness because of the assumption that the adsorbing layer has a density corresponding to a dense melt [44].

3.2. Characterization of extrudates

Extrudate quality depends on various extrusion process parameters. Shark skinning and melt fracture are among the most common surface defects that can develop during extrusion of soft polymers like PEO [45]. Shark skinning is a kind of surface defect that occurs due to molten polymer overflow. It happens at the point where the melt strength is surpassed by internal stresses. Melt fracture is the deterioration of the surface appearance. It tends to appear in high molecular weight PEO samples (beyond 600 kDa). In the current study, extrusion temperature and screw rate were initially varied to optimize extrudate quality. After various attempts, extrusion temperature was fixed at 80 °C and two extruder screw speeds were employed (30 and 90 rpm), which resulted in good extrudate quality (see Fig. 2).

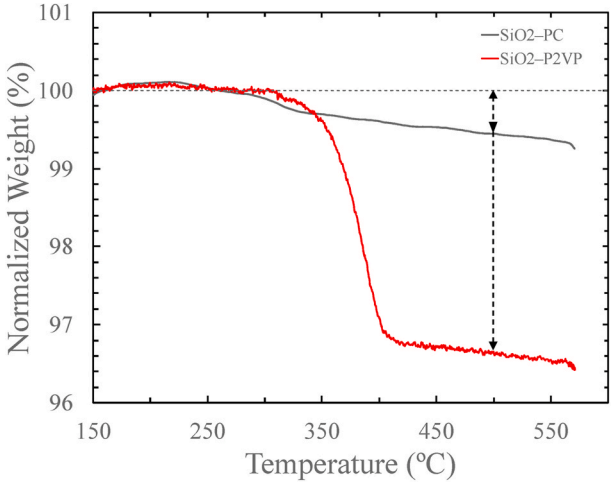

Fig. 1. Thermogravimetric analysis results of PC– and P2VP–adsorbed silica nanoparticles.

3.3. Nanoparticle dispersion

The microscopic morphology was first characterized by conducting SEM on cryo-fractured samples. Fig. 3 compares nanoparticle dispersion morphologies in various samples before and after extrusion at 30 rpm. Before extrusion, nanoparticles had a decent but not perfect dispersion; individual nanoparticles can be seen clearly on the SEM images. This observation is consistent with literature [18,21]. After extrusion at 80 °C and 30 rpm, large amount of agglomeration can be observed in all samples.

Unfortunately, SEM cannot provide the state of dispersion of nanofillers in 3-dimensional space. For this reason, SAXS experiments were performed on all samples to better quantify nanofiller dispersion. 1-dimensional (1D) SAXS patterns for all samples are presented in Fig. 4. Multiple Guinier and power law regions can be clearly seen in the 1D SAXS patterns, which indicates that our samples have a complex multiscale structure [46]. At high wavevectors ($q > 1/R_p$, where R_p is the radius of the primary particle), the signature of primary particles can be seen as a tiny shoulder with a power law tail associated with primary particle surface. The change in slope at intermediate wavevectors is attributed to agglomerates and is believed to be located around π/R_{agg}, where R_{agg} is the radius of the agglomerate [46].

1D SAXS patterns were analyzed and fitted by employing a 2-level unified model that was developed by Beaucage et al. [38]. The 2-level model used is applicable to a variety of complex systems that contain multiple levels of related structural features, in which each level is described by a Guinier and an associated power-law regime (see Eq. (3)). This method has been proven successful in unraveling multiscale structures over wavevector ranges of many orders of magnitude without introducing new parameters. The 2-level unified model fitting equation is given as follows:

$$I_i(q) = \sum_{i=1}^{2} G_i \exp\left(\frac{-q^2 R_{g,i}^2}{3}\right) + B_i \exp\left(\frac{-q^2 R_{g,i+1}^2}{3}\right) \left\{ \frac{\left[\operatorname{erf}\left(\frac{qR_{g,i}}{\sqrt{6}}\right)\right]^3}{q} \right\}^{P_i} \quad (3)$$

where i refers to the structure level (level 1 stands for primary particle, level 2 stands for non-fractal aggregation structure), G and B are fitting constants, R_g is the radius of gyration, and P_i is the packing factor of level i. The results of 2-level unified fittings are presented in Table 2. The first level packing factors for all samples were found to be close to four, which suggests that the surfaces of individual particles are sharp. According to the fitting results, the radius of primary silica particles range between 13 and 20 nm, which agrees well with our SEM results (Fig. 3) but smaller than the nominal size from the manufacturer. The primary particle size increased with the adsorption of high-T_g PC and P2VP chains. The primary particle size of the P2VP–adsorbed nanoparticles was greater than PC–adsorbed nanoparticles, which is consistent with the TGA results and work of adhesion ratio calculations and suggests that P2VP–SiO_2 interactions are stronger than PC–SiO_2. The larger primary particle size in the composites containing adsorbed polymers can be interpreted in many different ways. For example, the additional size of the coated particles could be a direct indication of the amount and thickness of P2VP or PC on the silica surface: ~6.0 nm for PC and ~6.9 nm for P2VP, which are at least ~10 times greater than those estimated from TGA experiments, but close to the R_g size of polymer chains (Table 1). Considering that SAXS analysis was performed on samples that contained the matrix polymer PEO, whereas TGA experiments were conducted in the absence of PEO (prior to mixing adsorbed nanoparticles with PEO), therefore, it is possible that the greater adsorbed layer thickness estimations obtained from the SAXS experiments might be due to the diffusion of PEO chains into the adsorbed layers [44].

The before and after extrusion fitting results showed differences in all

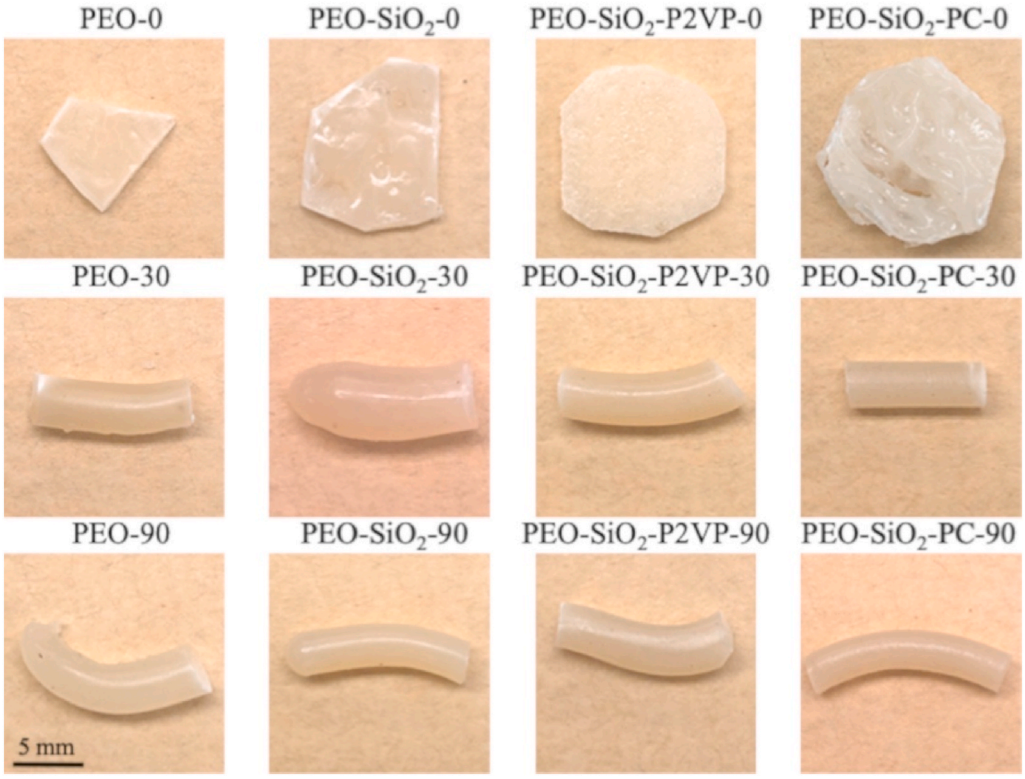

Fig. 2. Surface quality of various samples after extrusion. The top row shows unprocessed samples.

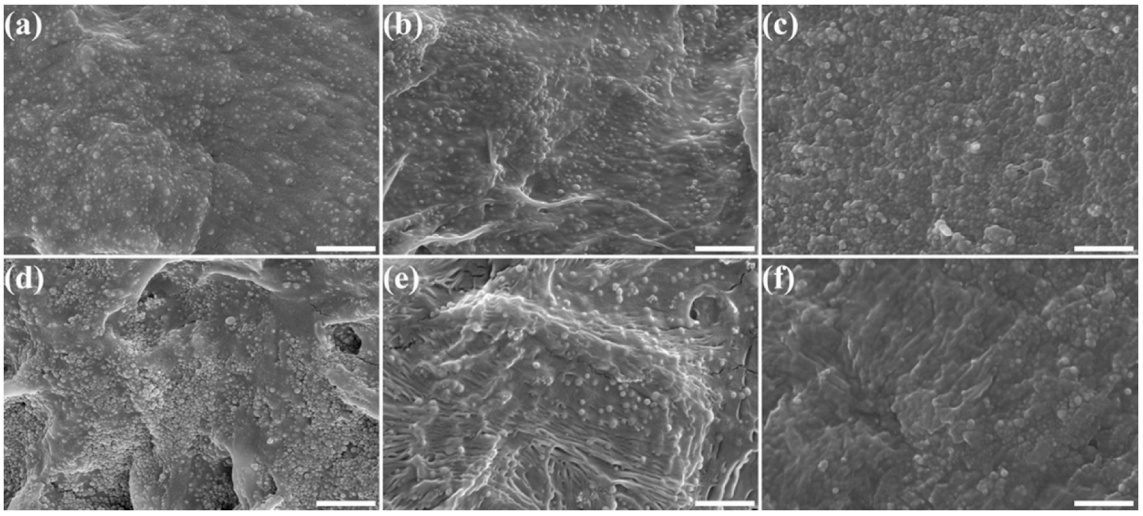

Fig. 3. SEM images of cryo-fractured nanocomposites of unprocessed samples (a–c) and samples extruded at 80 °C and 30 rpm (d–f). (a,d) PEO–SiO_2, (b,e) PEO–SiO_2–P2VP, (c,f) PEO–SiO_2–PC. Scale bar is equal to 1 μm.

systems. The primary particle size showed the greatest change especially for the composites containing PC and P2VP. The primary particle size decreased ~5.0 nm in the case of PEO–SiO_2–PC composites, and ~3.0 nm in the case of PEO–SiO_2–P2VP, whereas bare silica composite (PEO–SiO_2) only showed a decrease of ~0.35 nm, which was within the error. The significant changes observed in the primary particle sizes of the PEO–SiO_2–PC and PEO–SiO_2–P2VP composites could be attributed to the desorption of P2VP and PC chains from silica or to the de-mixing of PEO and adsorbed (P2VP and PC) chains. If the former mechanism is dominant, then loss of adsorbed chains should lead to a weakened interface and nanofiller agglomeration should be more pronounced. Whereas, if the latter mechanism is dominant, then the reinforced interface should act as a strong barrier against nanofiller agglomeration. By comparing the average aggregation radius R_2, it can also be concluded that PEO–SiO_2–P2VP composites tend to form larger aggregates, which is also due to the stronger interaction between P2VP and SiO_2.

Although SAXS is a powerful technique in measuring feature sizes, it has limited capability in counting the number of different microstructures. According to Hassinger et al. the descriptor with highest significance in depicting the microstructure is the total surface area of filler phase [43]. Intuitively, the formation of agglomerates would lead to a reduction in the nanofiller surface area exposed to matrix polymer, which will then lead to decreased level of confinement and increased

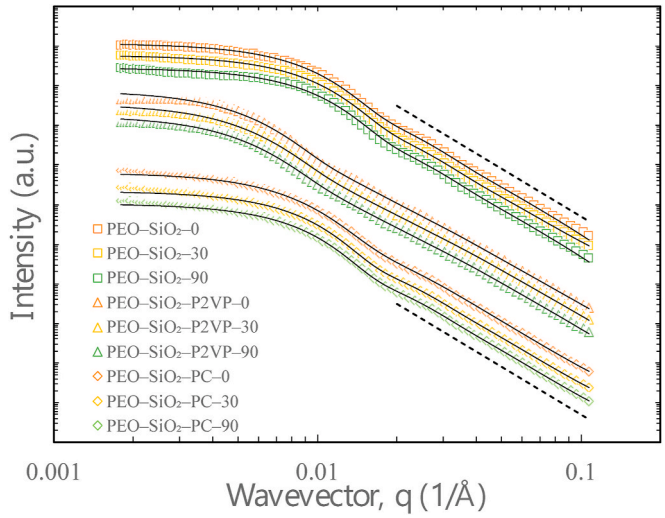

Fig. 4. Experimental SAXS spectra (symbols) and 2–level Unified model fitting results (solid black lines) for bare SiO_2, P2VP–adsorbed SiO_2, and PC–adsorbed SiO_2 containing PEO nanocomposites before (PEO–SiO_2–0, PEO–SiO_2–P2VP–0, and PEO–SiO_2–PC–0) and after (30 or 90 rpm) extrusion at 80 °C. The dashed lines have a slope of −4.

Table 2
SAXS fitting results for bulk nanocomposites using the 2-level unified model.

Sample	R_1 (nm)[a]	R_2 (nm)[a]	P_1
PEO–SiO_2–0	13.28 ± 0.44	30.46 ± 0.26	3.87
PEO–SiO_2–30	12.96 ± 0.58	29.49 ± 0.41	3.88
PEO–SiO_2–90	12.84 ± 0.70	29.12 ± 0.53	3.87
PEO–SiO_2–PC–0	19.23 ± 0.34	35.14 ± 0.24	4.00
PEO–SiO_2–PC–30	14.24 ± 0.57	32.25 ± 0.31	4.00
PEO–SiO_2–PC–90	14.20 ± 0.45	32.24 ± 0.23	4.00
PEO–SiO_2–P2VP–0	20.16 ± 2.06	52.22 ± 1.55	3.73
PEO–SiO_2–P2VP–30	17.04 ± 0.90	52.43 ± 1.68	3.77
PEO–SiO_2–P2VP–90	17.20 ± 0.70	53.36 ± 1.42	3.79

[a] The hydrodynamic radius, R, is related to radius of gyration, R_g, as follows: $R = R_g\sqrt{5/3}$.

free volume, hence might significantly alter the static and dynamic behavior of the nanocomposites. In this work, we propose two indirect ways to investigate the amount of agglomeration: (i) crystallization of PEO and (ii) amount of exposed silica surface groups. Crystallinity of PEO in PEO/SiO_2 nanocomposites was shown to inversely depend on silica concentration [47]. In the current study the concentration of silica is fixed, so we propose that the crystallinity of PEO actually depends on the amount of silica (or modified silica) it interacts with, and therefore, on the amount of silica surface (or modified silica surface) exposed to PEO. Crystallinity of PEO should then be related to the extent of agglomeration – a high amount of agglomeration would lead to less PEO–silica interactions and thereby, lead to greater PEO crystallinity. In addition to using PEO crystallinity as an indirect indicator of silica agglomeration, one can also use ATR-FTIR to measure the relative intensity (or peak area) of silica surface groups in various nanocomposites to that of PEO to obtain a quantitative comparison of the fraction of aggregated clusters. Given that the PEO concentration is fixed in all samples, the FTIR signature of neat PEO can be used as a benchmark for all other samples.

WAXS and ATR-FTIR experiment results are provided in Figs. 5 and 6, respectively. The results of PEO crystallinity (as obtained from WAXS experiments) and relative ATR-FTIR intensity of silica, which is calculated as the area ratio of the PEO peak at 840 cm^{-1} and silica peak at 790–800 cm^{-1}, are provided in Fig. 7. The crystallinity of neat PEO was the greatest among all samples and was measured to be 42.3% before

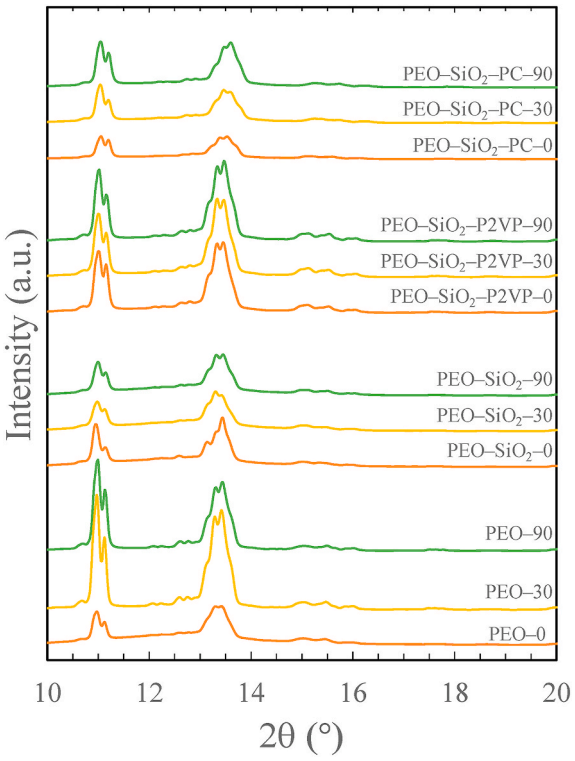

Fig. 5. Wide angle X–ray scattering results for neat PEO, PEO–SiO_2, PEO–SiO_2–PC, and PEO–SiO_2–P2VP.

extrusion, 47.5% after extrusion at 30 rpm, and 51.8% after extrusion at 90 rpm. The (relative) crystallinities of all samples are provided in Fig. 7a with respect to the crystallinity of neat PEO. In general, the relative crystallinities of nanocomposite samples were lower than that of neat PEO but, as expected, the lowest relative crystallinity was observed in the bare silica/PEO nanocomposites (PEO–SiO_2). In these samples, crystallization of PEO is affected by the presence of silica nanoparticles, which retard PEO chain dynamics and prevent formation of crystalline nuclei [48]. The amount of crystallinity in our PEO–SiO_2 samples agrees well with literature where the crystallinity of PEO was measured in confined PEO/silica networks at the same silica concentration as used in the current study [47]. The two nanocomposites with PC– and P2VP–adsorbed chains had greater crystallinities than the bare silica/-PEO nanocomposites. One possible explanation for this observation is the reduced number of PEO-silica contacts due to increased number of silica nanoparticle agglomerates. One can suggest that the presence of adsorbed layers alone could be used to explain the increased crystallinity in PEO–SiO_2–PC and PEO–SiO_2–P2VP nanocomposites, however, we argue against this suggestion because PEO has a higher affinity to P2VP and PC than it has to silica, therefore, although the adsorbed P2VP and PC layers would prevent PEO-silica interactions, they will also entangle with the PEO chains and prevent them from forming crystallites. Based on the surface energy arguments, we believe that the latter effect is stronger than the former, and therefore, the observed increase in PEO crystallinity in PC– and P2VP–adsorbed systems should be mostly attributed to increased amount of agglomeration in these systems. Finally, it is seen that PEO–SiO_2–P2VP has a greater crystallinity than PEO–SiO_2–PC. This observation actually agrees well with the SAXS results, which showed that PEO–SiO_2–P2VP nanocomposites have larger aggregates, and therefore, there are more primary silica particles occluded inside the larger aggregates found in PEO–SiO_2–P2VP system that are shielded from the PEO matrix. And as a result, the PEO chains are less likely to be interacting with silica nanoparticles, and thereby, more likely to be able to form crystallites.

The result of the relative FTIR peak ratio analysis is shown in Fig. 7b,

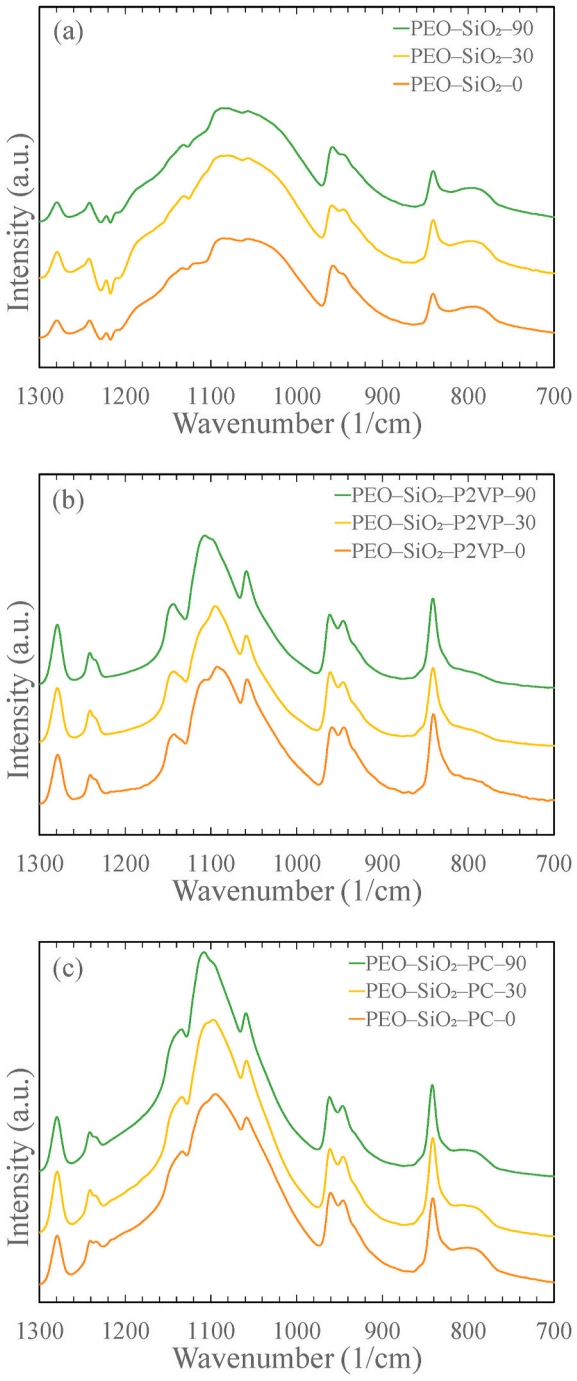

Fig. 6. ATR–FTIR spectrums of silica/PEO nanocomposites containing (a) bare silica (PEO–SiO_2) or silica covered with (b) P2VP (PEO–SiO_2–P2VP) or (c) PC (PEO–SiO_2–PC). Spectra were shifted vertically for better viewing. Peaks within the 750–850 cm^{-1} region are used to calculate relative peak area ratios as follows: $A_{SiO_2,790cm^{-1}}/A_{PEO,840cm^{-1}}$.

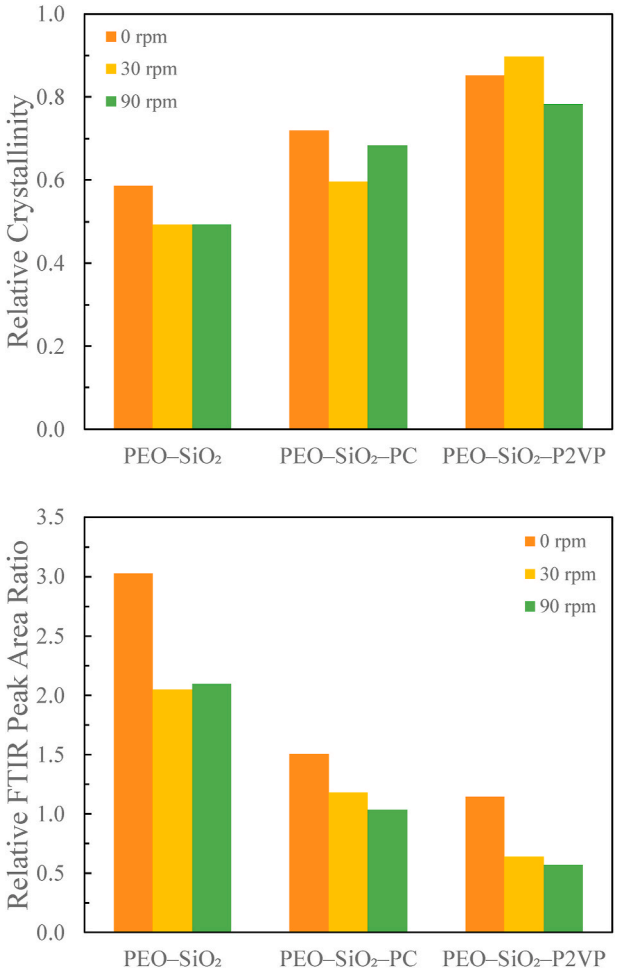

Fig. 7. Relative crystallinity and ATR–FTIR peak area ratio (A_{SiO2}/A_{PEO}) as a function of extrusion screw speed.

which suggests the same trend as the relative crystallinity results obtained from WAXS experiments. Bare SiO_2/PEO nanocomposite systems showed the greatest relative peak area ratios suggesting that they have the least number of silica agglomerates and possibly the least amount of clustering. On the other hand, the P2VP–adsorbed SiO_2/PEO nanocomposite system showed the smallest relative peak ratios suggesting that the P2VP–adsorbed SiO_2 composites have the greatest number of agglomerates and clustering among all the systems studied. Upon extrusion, ATR-FTIR peak ratios of PEO–SiO_2 and PEO–SiO_2–PC decreased by 31 and 32%, respectively, whereas that of PEO–SiO_2–P2VP was reduced by more than 50%. These results indicate that extrusion has a negative impact on the state of dispersion of nanoparticles. In general, the effect of extrusion showed the same trend in crystallinity and relative ATR-FTIR peak area ratios, however, the effect was clearer in the ATR-FTIR results. It is possible that the crystallinity results can be complicated by the PEO cleavage during extrusion. Upon extrusion, the relative FTIR peak area ratios decreased for all samples suggesting that processing led to increased amount of agglomeration and agrees with our SEM analysis results.

To summarize, the robustness of the particle dispersion to extrusion in PNCs with heterogeneous interfaces is not as good as those with homogeneous interfaces. The application of non-equilibrium processing increased the amount of agglomeration in the two PNC systems with heterogeneous interface, specifically, clustering after extrusion in PEO–SiO_2–P2VP has larger average size and population compared to PEO–SiO_2–PC. It is counterintuitive in some sense because extrusion was widely used to disperse nanofillers in PNCs. It can then be concluded that during the extrusion process, deagglomeration due to the large shear force and re-agglomeration due to the particle collision coexist and in PNCs with adsorbing polymer chains on fillers, re-agglomeration may dominate. Additionally, the larger and more clustering structure in PEO–SiO_2–P2VP can be ascribed to the stronger interaction between P2VP and SiO_2. And according to a recent study, the local viscosity around adsorbing P2VP is lower than that of PC because of its higher rigidity, which can also contribute to the formation of agglomeration [49].

3.4. Mechanical properties

Before understanding the influence of extrusion on nanocomposite mechanical properties, it is important to clarify the reinforcement mechanism. Chen et al. developed a parameter free analytic model to study the linear viscoelasticity of polymer nanocomposites [3]. They suggested that the reinforcement in a polymer nanocomposite can be described by two independent components arising from the polymer matrix and a percolated fractal nanoparticle structure formed by polymer chains acting as connecting bridges between nanoparticles. The main parameters that control the percolated fractal nanoparticle structure are nanoparticle size (radius, r) and nanofiller volume fraction (φ). Depending on the interplay between these two parameters, the percolated fractal nanoparticle structure could involve glassy polymeric bridges, rubbery polymeric bridges or no bridges. These three domains are separated from each other at two critical concentrations: φ^* and φ^{**}, which can be obtained as follows:

$$h_{near} = \begin{cases} b & \Rightarrow \quad \varphi^*(r,b) \\ R & \Rightarrow \quad \varphi^{**}(r,R) \end{cases} \tag{4}$$

where h_{near} is the average nearest neighbor distance between particles, b is the Kuhn length [50], and R is the average chain end-to-end distance. The average nearest neighbor distance between particles can be obtained by solving the following integral [3]:

$$h_{near} = 2re^{\frac{2\varphi}{1-\varphi^3}} \int_1^\infty e^{-4(1+\varphi)\left(x^3-1\right)+3\varphi(3+\varphi)\left(x^2-1\right)-6\varphi^2(x-1)} \mathrm{d}x \tag{5}$$

And for $\varphi > 0.2$, h_{near} can be approximated as follows [3]:

$$h_{near} \approx \frac{r(1-\varphi)^3}{6\varphi(2-\varphi)} \tag{6}$$

PEO has a Kuhn length of 0.67 nm and an average end-to-end distance of 41.91 nm. Therefore, φ^* and φ^{**} are calculated to be 0.51 and 0.044, respectively, for our nanocomposite systems by assuming an average particle radius (r) of 25 nm. The volume fraction of silica in bare silica/PEO composites (PEO–SiO_2) is ~0.17 (by volume) and falls in between the two critical concentrations, therefore, it can be concluded that rubbery bridges are responsible for most of the reinforcement in our samples according to this model.

Increasing temperature relaxes and softens the polymer bridges in network of composites. In our samples, the polymer bridges involve both matrix and adsorbed polymers and would be affected by the density of entanglements. The entanglements between matrix and adsorbed polymer chains are believed to be more persistent when temperature is greater than the glass transition temperatures of both polymers and may lead to stiffening behavior as shown in PEO and PMA nanocomposite systems [18,19]. However, in the current study, both extrusion processing and viscoelastic analysis was performed at temperatures below the T_g of the adsorbed polymers, therefore, we do not expect to see thermal stiffening. On the other hand, we expect chain breaking due to thermal degradation and rearrangement of rubbery bridges due to agglomeration of silica nanoparticles and due to high shear rates during extrusion [45].

Frequency sweep experiments were conducted to investigate the frequency dependency of viscoelastic properties of our nanocomposites. The controlled strain was set within the linear region (0.5%), and experiments were performed at 85 °C, which is greater than the T_g of PEO but lower than the T_gs of P2VP and PC. The frequency sweep results are presented in Fig. 8. The storage (G') and loss (G'') moduli of nanocomposites were quite different from those of neat PEO, and the viscoelastic behavior of all samples was affected by extrusion. It is interesting to see that even in neat PEO samples, a certain degree of decrease in both G' and G'' took place after extrusion, which is partially attributed to the

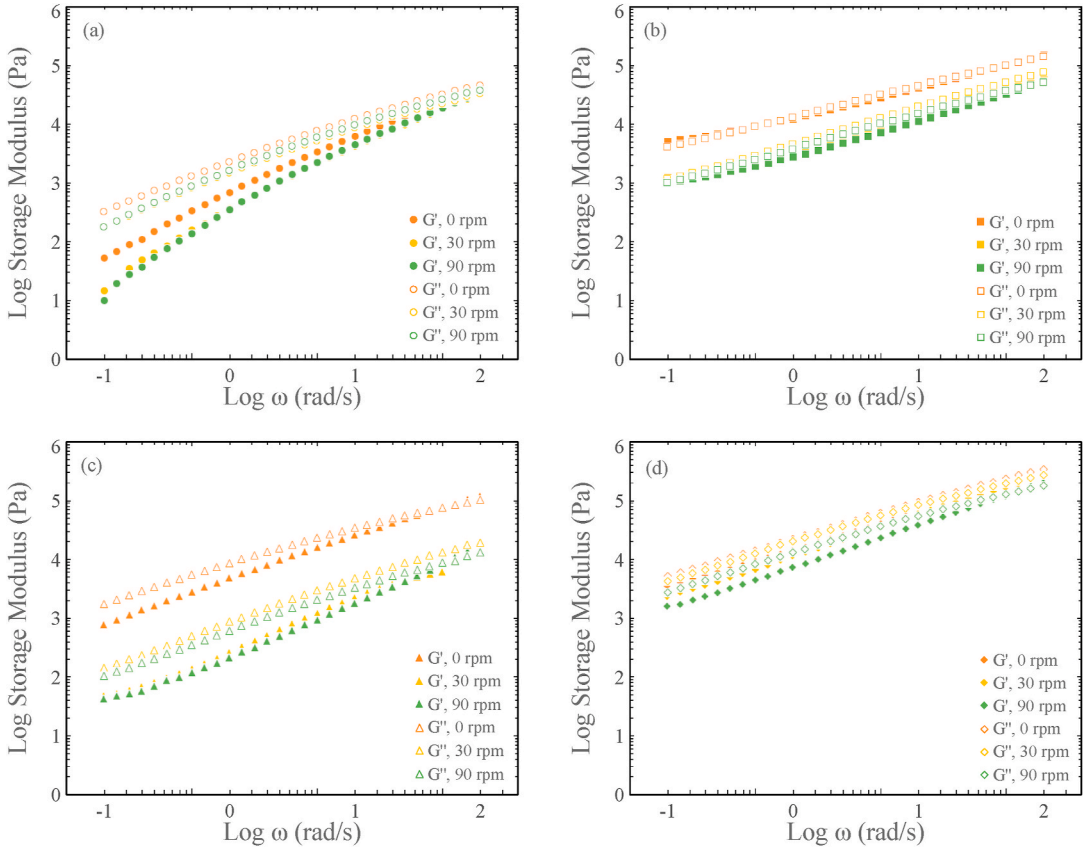

Fig. 8. Frequency sweep results of (a) neat PEO, (b) PEO–SiO_2, (c) PEO–SiO_2–P2VP, and (d) PEO–SiO_2–PC at 0.5% strain and 85 °C.

thermal degradation of PEO chains during melt extrusion [51]. Neat PEO samples' G' and G'' showed terminal relaxation at low frequency, which indicates a liquid–like behavior. In contrast, nanocomposite samples became less dependent on frequency at low frequencies, and they showed a transition towards plateau behavior, which is an indication of a gel–like network formation.

PEO–SiO_2, PEO–SiO_2–P2VP, and PEO–SiO_2–PC all had greater G' and G'' compared to neat PEO. Considering the amount of silica nanoparticles present in the matrix (30% by weight), the reinforcement is believed to be largely due to the formation of a network that is composed of nanoparticles connected by matrix and adsorbed chains (when adsorbed chains are present). The unprocessed samples were shown to have a relatively uniform nanoparticle dispersion, and therefore, it is assumed that the polymer chain bridges are better extended throughout the sample. Whereas after extrusion, the situation became quite different. PEO–SiO_2 and, especially, PEO–SiO_2–P2VP showed a drastic decrease in both G' and G'' upon extrusion, whereas PEO–SiO_2–PC retained most of its G' and G''. To quantify the reinforcement effect in different nanocomposite systems, the G' plateau at low frequency, $G'_{plateau}$ was used as a descriptor. For PEO–SiO_2 and PEO–SiO_2–P2VP, the ratio of $G'_{plateau}$ before and after extrusion, $G'_{plateau}(90\ rpm)/G'_{plateau}(0\ rpm)$ are 0.19 and 0.064, respectively, where the ratio for PEO–SiO_2–PC is 0.51. In terms of microstructure, bare PEO–SiO_2 nanocomposites showed agglomeration, as shown in SEM images of Fig. 3, which is believed to be the main reason for the observed degradation of its viscoelastic properties. PEO–SiO_2–P2VP nanocomposites had the largest agglomerates before extrusion as indicated by R_2 values (Table 2), which maintained their size after extrusion. In addition, these nanocomposites also showed the greatest amount of agglomeration based on WAXS and ATR-FTIR analysis. In the case of PEO–SiO_2–P2VP, it can be seen that a reduction in nanoparticle surface area by 50% (calculated from ART-FTIR results) lead to a reduction in $G'_{plateau}$ by as large as ~93%, whereas in PEO–SiO_2–PC, a reduction in nanoparticle surface area by 32% lead to a reduction in $G'_{plateau}$ by 49%. On the other hand, the average size of agglomerates in PEO–SiO_2–PC nanocomposites slightly decreased upon extrusion which was accompanied by a modest increase in the amount of agglomeration (compared to PEO–SiO_2 and PEO–SiO_2–P2VP), and therefore, it is suggested that the average interparticle distance in these nanocomposites remained mostly unchanged and the flexible bridges that were present before extrusion were still mostly intact after extrusion.

Processing might also affect the state of de-mixing and de-entanglement at the chemical heterogeneous interface. However, if the effect of deformation on the interface can be healed within the time domain of the extrusion processing then deformed samples could still retain their pre-deformed viscoelastic properties. PC chains are more flexible when mixing with PEO compared to P2VP chains, and therefore, they are more likely to recover and re-entangle with matrix PEO chains quicker than P2VP chains [52]. The difference in interface stiffness not only affects the structure of the adsorbed polymer layer but also the chain dynamics of the adsorbed polymer layer. Carrillo et al. showed that in polymer nanocomposites tails and train segments are more prevalent for rigid polymers while loops are more dominant for flexible polymers [53]. Therefore, segmental dynamics should be slower for stiffer chains due to the densification and a more persistent layering of chain segments in the adsorbed polymer layer. As a result, for example, when P2VP–coated silica nanoparticles aggregate due to shearing against each other during extrusion, they form a stiffer entangled interface between the newly agglomerated nanofillers compared to PC–coated silica fillers. Therefore, agglomerates formed by P2VP–coated nanofillers are more resistant to further change compared to agglomerates formed in PC–coated nanofillers because overlapping PC layers on neighboring nanoparticles can relax and disentangle from each other due to the higher flexibility of PC chains.

Surface modification of nanofillers has been proven to be a feasible way to reduce interfacial tension and improve the state of dispersion and distribution of nanofillers [54]. As for silica nanoparticles, silanes or oligomers can be attached to the surface via chemical or physical reactions, and nanocomposites based on these modified silica nanoparticles usually achieve better dispersion upon compounding [13,43,55]. However, as demonstrated by SEM, ATR-FTIR, and WAXS experiments, the nanocomposites used in the current study did not benefit from extrusion processing even though nanofiller dispersion was theoretically predicted to be uniform. SAXS results suggested an adsorbed layer thickness of 6–7 nm, which is much larger than the thicknesses that can be achieved with silane or oligomeric modifiers (which in many cases is less than 1 nm). The physically adsorbed polymer layers can be viewed as thick and loosely packed regions, and as a result, modified nanoparticles behave like "sticky" nanofillers with definite dynamic scoping – they can disperse in solution or polymer matrix and form stable solutions and composites, however, collisions between the sticky nanofillers lead to irreversible clustering. Therefore, when encountered with shear fields during non–equilibrium processing, these nanocomposites with "sticky" nanoparticles tend to form agglomerates.

4. Conclusions

In the current study, the influence of extrusion processing on the structure and viscoelastic properties of two dynamically heterogeneous polymer nanocomposites were investigated. The results were compared to those of bare nanofiller containing nanocomposite and neat matrix polymer. Poly(ethylene oxide), PEO, was the matrix polymer and colloidal silica (SiO_2) was the nanofiller in all systems. The two heterogeneous polymer nanocomposites contained physically adsorbed polymers: poly(2–vinyl pyridine), P2VP, or poly(carbonate), PC. Both P2VP and PC have glass transition temperatures greater than that of PEO, and therefore, they offer different levels of dynamic asymmetry at interfaces anchored by silica nanofillers. The experimental results led to the following conclusions:

1. All three nanocomposites (PEO–SiO_2, PEO–SiO_2–P2VP, and PEO–SiO_2–PC) showed decent state of dispersion prior to processing. Upon processing, all three nanocomposites showed some degree of agglomeration. The agglomeration in PEO–SiO_2 can be well captured by established models for predicting dispersion state after extrusion, however, the two heterogeneous nanocomposite systems (PEO–SiO_2–P2VP and PEO–SiO_2–PC) showed agglomeration behavior contradictory to the models. The existence of heterogeneous interface makes the nanocomposite distinct from traditional binary nanocomposites.
2. Agglomeration clusters can be clearly visualized in SEM images of post-extrusion samples. The average sizes of microstructures at different length scales were quantified via small angle X-ray scattering experiments. PEO–SiO_2–P2VP nanocomposites showed the largest agglomerations, which may due to the better affinity of P2VP to SiO_2 nanoparticles. Fractal structures may form at larger length scales, however, the q-range of the current SAXS experiments is not sufficient to capture information at length scales greater than $q = 0.003\ \mathring{A}^{-1}$. USAXS experiments and a more thorough analysis will be performed in future studies.
3. The adsorbed polymers were instrumental in separating the matrix PEO chains and silica nanofillers from each other, and as a result, the crystallinity of PEO in the heterogeneous nanocomposites (PEO–SiO_2–P2VP and PEO–SiO_2–PC) was greater than the crystallinity of PEO in PEO–SiO_2, where PEO matrix chains interact directly with the silica nanofillers, and therefore, display lower crystallinity. All three nanocomposite systems had lower crystallinity than the neat PEO before extrusion. Upon extrusion, the relative crystallinity in all three nanocomposites systems decreased, which was attributed

to the formation of agglomerates upon extrusion. Agglomeration reduces the amount of silica surface that matrix PEO chains might be exposed to, and thereby, leads to higher crystallinity. In addition, agglomeration should also lead to a decreased amount of PEO and adsorbed polymer interactions, which should also positively impact the crystallinity of matrix PEO chains. In general, extrusion led to a decreased crystallinity in all nanocomposite samples as compared to the crystallinity of neat PEO under the same extrusion conditions. This was used as an indirect indicator of the increased amount of agglomeration in the processed nanocomposites.

4. Attenuated total reflectance-Fourier transform infrared (ATR-FTIR) spectra experiments were used to calculate relative amount of exposed silica surface groups in different samples. ATR-FTIR relative peak area ratio analysis results support conclusions derived from crystallinity analysis. Bare SiO_2/PEO nanocomposites (PEO–SiO_2) showed the greatest relative peak area ratios suggesting that they have the least amount of silica agglomerates. On the other hand, the P2VP-adsorbed SiO_2/PEO nanocomposites showed the smallest relative peak ratios suggesting that the P2VP-adsorbed SiO_2 composites have the greatest number of agglomerates among all the systems studied.
5. The viscoelastic properties were investigated via strain controlled oscillatory rheology experiments. Extrusion led to degradation of the storage modulus of all samples, however this effect was most obvious in bare silica (PEO–SiO_2) and P2VP–adsorbed silica (PEO–SiO_2–P2VP) containing nanocomposites. The reduction in nanocomposite reinforcement is partially related to agglomeration after extrusion, which breaks the polymer bridges connecting percolated nanoparticle network. It is also attributed to the desorption and disentanglement within the heterogeneous interface, which also leads to destruction of the polymeric bridges. The drastic difference in the viscoelastic behavior of the P2VP- and PC-adsorbed systems strongly suggest that interfacial dynamics must be taken into account when designing polymer nanocomposites with dynamically asymmetric, heterogeneous interfaces.

Declaration of competing interest

The authors declare that they have no known competing financial interests or personal relationships that could have appeared to influence the work reported in this paper.

Acknowledgements

This material is based upon work supported by the National Science Foundation CMMI MEP program under Grant Nos. 1825250 (Akcora) and 1825254 (Ozisik).

Appendix A. Supplementary data

Supplementary data to this article can be found online at https://doi.org/10.1016/j.polymer.2021.123813.

References

[1] P. Akcora, S.K. Kumar, J. Moll, S. Lewis, L.S. Schadler, Y. Li, B.C. Benicewicz, A. Sandy, S. Narayanan, J. Ilavsky, P. Thiyagarajan, R.H. Colby, J.F. Douglas, "Gel-like" mechanical reinforcement in polymer nanocomposite melts, Macromolecules 43 (2010) 1003–1010, https://doi.org/10.1021/ma902072d.
[2] Y. Song, Q. Zheng, Concepts and conflicts in nanoparticles reinforcement to polymers beyond hydrodynamics, Prog. Mater. Sci. 84 (2016) 1–58, https://doi.org/10.1016/j.pmatsci.2016.09.002.
[3] Q. Chen, S. Gong, J. Moll, D. Zhao, S.K. Kumar, R.H. Colby, Mechanical reinforcement of polymer nanocomposites from percolation of a nanoparticle network, ACS Macro Lett. 4 (2015) 398–402, https://doi.org/10.1021/acsmacrolett.5b00002.
[4] S. Cheng, V. Bocharova, A. Belianinov, S. Xiong, A. Kisliuk, S. Somnath, A.P. Holt, O.S. Ovchinnikova, S. Jesse, H. Martin, T. Etampawala, M. Dadmun, A.P. Sokolov, Unraveling the mechanism of nanoscale mechanical reinforcement in glassy polymer nanocomposites, Nano Lett. 16 (2016) 3630–3637, https://doi.org/10.1021/acs.nanolett.6b00766.
[5] Q. Zhang, L.A. Archer, Poly(ethylene oxide)/silica Nanocomposites: structure and rheology, Langmuir 18 (2002) 10435–10442, https://doi.org/10.1021/la026338j.
[6] S.K. Kumar, B.C. Benicewicz, R.A. Vaia, K.I. Winey, 50th anniversary perspective: are polymer nanocomposites practical for applications? Macromolecules 50 (2017) 714–731, https://doi.org/10.1021/acs.macromol.6b02330.
[7] R.D. Priestley, C.J. Ellison, L.J. Broadbelt, J.M. Torkelson, Structural relaxation of polymer glasses at surfaces, interfaces, and in between, Science 309 (2005) 456–459, https://doi.org/10.1126/science.1112217.
[8] L.S. Schadler, S.K. Kumar, B.C. Benicewicz, S.L. Lewis, S.E. Harton, Designed interfaces in polymer nanocomposites: a fundamental viewpoint, MRS Bull. 32 (2007) 335–340, https://doi.org/10.1557/mrs2007.232.
[9] E. Senses, P. Akcora, An interface-driven stiffening mechanism in polymer nanocomposites, Macromolecules 46 (2013) 1868–1874, https://doi.org/10.1021/ma302275f.
[10] S. Cheng, A.P. Holt, H. Wang, F. Fan, V. Bocharova, H. Martin, T. Etampawala, B. T. White, T. Saito, N.-G. Kang, M.D. Dadmun, J.W. Mays, A.P. Sokolov, Unexpected molecular weight effect in polymer nanocomposites, Phys. Rev. Lett. 116 (2016), 038302, https://doi.org/10.1103/PhysRevLett.116.038302.
[11] H. Mortazavian, C.J. Fennell, F.D. Blum, Structure of the interfacial region in adsorbed poly(vinyl acetate) on silica, Macromolecules 49 (2016) 298–307, https://doi.org/10.1021/acs.macromol.5b02214.
[12] N. Jiang, M. Sen, M.K. Endoh, T. Koga, E. Langhammer, P. Bjöörn, M. Tsige, Thermal properties and segmental dynamics of polymer melt chains adsorbed on solid surfaces, Langmuir 34 (2018) 4199–4209, https://doi.org/10.1021/acs.langmuir.8b00122.
[13] B. Natarajan, Y. Li, H. Deng, L.C. Brinson, L.S. Schadler, Effect of interfacial energetics on dispersion and glass transition temperature in polymer nanocomposites, Macromolecules 46 (2013) 2833–2841, https://doi.org/10.1021/ma302281b.
[14] X. Huang, C.B. Roth, Optimizing the grafting density of tethered chains to alter the local glass transition temperature of polystyrene near silica substrates: the advantage of mushrooms over brushes, ACS Macro Lett. 7 (2018) 269–274, https://doi.org/10.1021/acsmacrolett.8b00019.
[15] S.K. Kumar, N. Jouault, B. Benicewicz, T. Neely, Nanocomposites with polymer grafted nanoparticles, Macromolecules 46 (2013) 3199–3214, https://doi.org/10.1021/ma4001385.
[16] J.F. Moll, P. Akcora, A. Rungta, S. Gong, R.H. Colby, B.C. Benicewicz, S.K. Kumar, Mechanical reinforcement in polymer melts filled with polymer grafted nanoparticles, Macromolecules 44 (2011) 7473–7477, https://doi.org/10.1021/ma201200m.
[17] M.S. Nikolic, C. Olsson, A. Salcher, A. Kornowski, A. Rank, R. Schubert, A. Frömsdorf, H. Weller, S. Förster, Micelle and vesicle formation of amphiphilic nanoparticles, Angew. Chem. Int. Ed. 48 (2009) 2752–2754, https://doi.org/10.1002/anie.200805158.
[18] E. Senses, A. Isherwood, P. Akcora, Reversible thermal stiffening in polymer nanocomposites, ACS Appl. Mater. Interfaces 7 (2015) 14682–14689, https://doi.org/10.1021/acsami.5b02046.
[19] E. Senses, A. Faraone, P. Akcora, Microscopic chain motion in polymer nanocomposites with dynamically asymmetric interphases, Sci. Rep. 6 (2016) 29326, https://doi.org/10.1038/srep29326.
[20] S. Yang, S. Liu, S. Narayanan, C. Zhang, P. Akcora, Chemical heterogeneity in interfacial layers of polymer nanocomposites, Soft Matter 14 (2018) 4784–4791, https://doi.org/10.1039/C8SM00663F.
[21] S. Yang, M. Hassan, P. Akcora, Role of adsorbed chain rigidity in reinforcement of polymer nanocomposites, J. Polym. Sci., Part B: Polym. Phys. 57 (2019) 9–14, https://doi.org/10.1002/polb.24751.
[22] S. Yang, P. Akcora, Deformation of chemically heterogeneous interfacial layers of polymer nanocomposites, ACS Macro Lett. (2019) 1635–1641, https://doi.org/10.1021/acsmacrolett.9b00821.
[23] W. Gacitua, A. Ballerini, J. Zhang, Polymer nanocomposites: synthetic and natural fillers A review, Maderas Cienc. Tecnol. 7 (2005) 159–178, https://doi.org/10.4067/S0718-221X2005000300002.
[24] O. Cantin, F. Siepmann, F. Danede, J.F. Willart, Y. Karrout, J. Siepmann, PEO hot melt extrudates for controlled drug delivery: importance of the molecular weight, J. Drug Deliv. Sci. Technol. 36 (2016) 130–140, https://doi.org/10.1016/j.jddst.2016.09.003.
[25] E. Senses, P. Akcora, Mechanistic model for deformation of polymer nanocomposite melts under large amplitude shear, J. Polym. Sci., Part B: Polym. Phys. 51 (2013) 764–771, https://doi.org/10.1002/polb.23247.
[26] I. Alig, P. Pötschke, D. Lellinger, T. Skipa, S. Pegel, G.R. Kasaliwal, T. Villmow, Establishment, morphology and properties of carbon nanotube networks in polymer melts, Polymer 53 (2012) 4–28, https://doi.org/10.1016/j.polymer.2011.10.063.
[27] F.W. Starr, J.F. Douglas, S.C. Glotzer, Origin of particle clustering in a simulated polymer nanocomposite and its impact on rheology, J. Chem. Phys. 119 (2003) 1777–1788, https://doi.org/10.1063/1.1580099.
[28] A.C. Balazs, T. Emrick, T.P. Russell, Nanoparticle polymer composites: where two small worlds meet, Science 314 (2006) 1107–1110, https://doi.org/10.1126/science.1130557.
[29] J. Brus, J. Dybal, P. Schmidt, J. Kratochvíl, J. Baldrian, Order and mobility in Polycarbonate−Poly(ethylene oxide) blends studied by solid-state NMR and other techniques, Macromolecules 33 (2000) 6448–6459, https://doi.org/10.1021/ma000533s.

[30] C.-L. Yeh, T. Hou, H.-L. Chen, L.-Y. Yeh, F.-C. Chiu, A.J. Müller, N. Hadjichristidis, Lower critical ordering transition of poly(ethylene oxide)- *block* -poly(2-vinylpyridine), Macromolecules 44 (2011) 440–443, https://doi.org/10.1021/ma102322w.
[31] D. Janssen, R. De Palma, S. Verlaak, P. Heremans, W. Dehaen, Static solvent contact angle measurements, surface free energy and wettability determination of various self-assembled monolayers on silicon dioxide, Thin Solid Films 515 (2006) 1433–1438, https://doi.org/10.1016/j.tsf.2006.04.006.
[32] D. Aronov, G. Rosenman, Surface energy modification by electron beam, Surf. Sci. 601 (2007) 5042–5049, https://doi.org/10.1016/j.susc.2007.09.003.
[33] L. Duta, A.C. Popescu, I. Zgura, N. Preda, I.N. Mihailescu, Wettability of Nanostructured Surfaces, Wetting Wettability, 2015, https://doi.org/10.5772/60808.
[34] F. Zhang, J. Ilavsky, G.G. Long, J.P.G. Quintana, A.J. Allen, P.R. Jemian, Glassy carbon as an absolute intensity calibration standard for small-angle scattering, Metall. Mater. Trans. 41 (2010) 1151–1158, https://doi.org/10.1007/s11661-009-9950-x.
[35] J. Ilavsky, Nika: software for two-dimensional data reduction, J. Appl. Crystallogr. 45 (2012) 324–328, https://doi.org/10.1107/S0021889812004037.
[36] J. Ilavsky, P.R. Jemian, Irena: tool suite for modeling and analysis of small-angle scattering, J. Appl. Crystallogr. 42 (2009) 347–353, https://doi.org/10.1107/S0021889809002222.
[37] A. Nelson, Co-refinement of multiple-contrast neutron/X-ray reflectivity data using MOTOFIT, J. Appl. Crystallogr. 39 (2006) 273–276, https://doi.org/10.1107/S0021889806005073.
[38] G. Beaucage, Approximations leading to a unified exponential/power-law approach to small-angle scattering, J. Appl. Crystallogr. 28 (1995) 717–728, https://doi.org/10.1107/S0021889895005292.
[39] JADE for XRD, (n.d.). https://materialsdata.com/prodjd.html. (Accessed 17 November 2020).
[40] K.W. Stöckelhuber, A. Das, R. Jurk, G. Heinrich, Contribution of physico-chemical properties of interfaces on dispersibility, adhesion and flocculation of filler particles in rubber, Polymer 51 (2010) 1954–1963, https://doi.org/10.1016/j.polymer.2010.03.013.
[41] F.M. Fowkes, Attractive forces at interfaces, Ind. Eng. Chem. 56 (1964) 40–52, https://doi.org/10.1021/ie50660a008.
[42] V. Ganesan, C.J. Ellison, V. Pryamitsyn, Mean-field models of structure and dispersion of polymer-nanoparticle mixtures, Soft Matter 6 (2010) 4010, https://doi.org/10.1039/b926992d.
[43] I. Hassinger, X. Li, H. Zhao, H. Xu, Y. Huang, A. Prasad, L. Schadler, W. Chen, L. Catherine Brinson, Toward the development of a quantitative tool for predicting dispersion of nanocomposites under non-equilibrium processing conditions, J. Mater. Sci. 51 (2016) 4238–4249, https://doi.org/10.1007/s10853-015-9698-1.
[44] N. Jouault, J.F. Moll, D. Meng, K. Windsor, S. Ramcharan, C. Kearney, S.K. Kumar, Bound polymer layer in nanocomposites, ACS Macro Lett. 2 (2013) 371–374, https://doi.org/10.1021/mz300646a.
[45] O. Cantin, PEO Hot Melt Extrudates for Controlled Drug Delivery, Human Health and Pathology, Université du Droit et de la Santé-Lille II, 2016.
[46] G.P. Baeza, A.-C. Genix, C. Degrandcourt, L. Petitjean, J. Gummel, M. Couty, J. Oberdisse, Multiscale filler structure in simplified industrial nanocomposite silica/SBR systems studied by SAXS and TEM, Macromolecules 46 (2013) 317–329, https://doi.org/10.1021/ma302248p.
[47] S. Jiang, D. Yu, X. Ji, L. An, B. Jiang, Confined crystallization behavior of PEO in silica networks, Polymer 41 (2000) 2041–2046, https://doi.org/10.1016/S0032-3861(99)00342-0.
[48] A.J. Waddon, Z.S. Petrovic, Spherulite crystallization in poly(ethylene oxide)–silica nanocomposites. Retardation of growth rates through reduced molecular mobility, Polym. J. 34 (2002) 876–881, https://doi.org/10.1295/polymj.34.876.
[49] D. Wu, D.G. Weiblen, R. Ozisik, P. Akcora, Local viscosity of interfacial layers in polymer nanocomposites measured by magnetic heating, ACS Appl. Polym. Mater. (2020), 0c00889, https://doi.org/10.1021/acsapm.0c00889 acsapm.
[50] P.J. Flory, J.G. Jackson, Statistical Mechanics of Chain Molecules, Hanser Publishers, 1989. https://books.google.com/books?id=6P5xQgAACAAJ.
[51] P. Malik, M. Castro, C. Carrot, Thermal degradation during melt processing of poly (ethylene oxide), poly(vinylidenefluoride-Co-Hexafluoropropylene) and their blends in the presence of additives, for conducting applications, Polym. Degrad. Stabil. 91 (2006) 634–640, https://doi.org/10.1016/j.polymdegradstab.2005.01.020.
[52] M. Tsuburaya, H. Saito, Crystallization of polycarbonate induced by spinodal decomposition in polymer blends, Polymer 45 (2004) 1027–1032, https://doi.org/10.1016/j.polymer.2003.11.026.
[53] J.-M.Y. Carrillo, S. Cheng, R. Kumar, M. Goswami, A.P. Sokolov, B.G. Sumpter, Untangling the effects of chain rigidity on the structure and dynamics of strongly adsorbed polymer melts, Macromolecules 48 (2015) 4207–4219, https://doi.org/10.1021/acs.macromol.5b00624.
[54] M. Wang, Developing bioactive composite materials for tissue replacement, Biomaterials 24 (2003) 2133–2151, https://doi.org/10.1016/S0142-9612(03)00037-1.
[55] R. Qiao, H. Deng, K.W. Putz, L.C. Brinson, Effect of particle agglomeration and interphase on the glass transition temperature of polymer nanocomposites, J. Polym. Sci., Part B: Polym. Phys. 49 (2011) 740–748, https://doi.org/10.1002/polb.22236.